

# Complexity of quantum tomography from genuine non-Gaussian entanglement

Received: 27 May 2025

Accepted: 21 November 2025

Published online: 05 December 2025

 Check for updatesXiaobin Zhao<sup>1</sup>✉, Pengcheng Liao<sup>1</sup>, Francesco Anna Mele<sup>2</sup>,  
Ulysse Chabaud<sup>3</sup> & Quntao Zhuang<sup>1,4</sup>✉

Quantum state tomography typically requires exponentially many copies of a quantum state, due to the complex correlations present in large systems. We show that, for bosonic systems, the scaling is completely determined by the nature of these correlations. Motivated by the Hong-Ou-Mandel effect and boson sampling, we define Gaussian-entangleable (GE) states, produced by generalized interference between separable bosonic modes. GE states greatly extend the Gaussian family, encompassing separable states, multi-mode Gottesman-Kitaev-Preskill codes, entangled cat states, and boson-sampling outputs—resources for error correction and quantum advantage. We prove that any pure GE state of  $m$  modes can be learned efficiently, requiring only  $\text{poly}(m)$  copies, via a protocol based on Gaussian unitaries, local tomography, and classical post-processing; for boson-sampling states, no Gaussian unitaries are needed. For states outside GE, we define an operational monotone—the minimal number of ancillary modes needed to make them GE—which exactly characterizes the exponential tomography overhead. We also show that deterministic generation of NOON states with  $N \geq 3$  via two-mode interference is impossible.

Quantum state tomography<sup>1–3</sup> aims to provide a classical description of quantum states from experimental data. As a fundamental task in physics and quantum information processing, it not only facilitates the tests of quantum physics, but also enables quantum device certification and benchmarking<sup>4</sup>. However, quantum state tomography is a challenging task in general—each measurement requires a new copy of the state as measurement collapses the original quantum state. To learn an approximate description of a quantum system with  $n$  qubits, the required number of samples is exponential in  $n$ <sup>5,6</sup>. In the case of bosonic systems, the infinite-dimensional Hilbert space casts additional challenges to the problem of tomography<sup>7</sup>.

The challenge in quantum state tomography arises from the complex nature of quantum correlations between subsystems: highly entangled states involving superpositions of a large number of states are generally hard to learn, while separable states with classical correlations are naturally easier to learn. At the same time, one may

identify subsets of non-separable quantum states that are easier to learn. For instance, refs. 7–9 developed efficient learning protocols for Gaussian bosonic quantum states<sup>10,11</sup>—a family of experimentally friendly states—and its generalization of  $t$ -doped Gaussian states. Thus, the interplay between properties of quantum correlation and learning sample complexity in bosonic quantum systems is unclear. In this work, we approach the problem by considering how quantum correlations are generated from separable states.

We begin by considering the example of the Hong–Ou–Mandel (HOM) effect<sup>12</sup>, where two incoming identical and separable single photons interfere on a beam-splitter to deterministically generate an entangled output, manifesting a bunching effect between indistinguishable photons. The output state  $\sim |20\rangle + |02\rangle$  is the  $N=2$  case of the family of NOON states  $\sim |N0\rangle + |0N\rangle$ , which are maximally entangled  $N$ -photon states useful to enhance quantum metrology<sup>13,14</sup>. Similar to HOM, in boson sampling experiments<sup>15</sup>, multiple modes of photons

<sup>1</sup>Ming Hsieh Department of Electrical and Computer Engineering, University of Southern California, Los Angeles, CA, USA. <sup>2</sup>Scuola Normale Superiore, Pisa, Italy. <sup>3</sup>DIENS, École Normale Supérieure, PSL University, CNRS, INRIA, Paris, France. <sup>4</sup>Department of Physics and Astronomy, University of Southern California, Los Angeles, CA, USA. ✉e-mail: [xzhao721@usc.edu](mailto:xzhao721@usc.edu); [qzhuang@usc.edu](mailto:qzhuang@usc.edu)

interfere on a network of beam-splitters creating highly multipartite entangled states, whose measurement statistics are hard to simulate classically, creating an opportunity to demonstrate quantum advantage<sup>16,17</sup>.

Inspired by the HOM effect<sup>12</sup> and boson sampling experiments<sup>15</sup>, we define Gaussian-entangleable (GE) states as states produced by generalized interference described by Gaussian processes<sup>10</sup> between separable bosonic modes (see Fig. 1). Despite the fact that GE states enable quantum computational advantage, we prove that an  $m$ -mode pure GE state is learnable with only  $\text{poly}(m)$  samples, by providing an explicit protocol—Gaussian disentangling (GDE) tomography—involving only Gaussian unitary, local tomography (e.g., homodyne or heterodyne) and classical processing. The protocol is robust to experimental imperfections, including weak loss and noise, and arbitrary homogeneous loss. We provide numerical simulations for learning the states generated from passing number states, cat states and thermal states over a lossy beam-splitter, demonstrating GDE’s advantage over conventional approaches.

For non-GE states, we derive an operation-driven monotone—the number of additional modes necessary to reduce them to GE states. Moreover, we prove that this monotone exactly captures the exponential overhead in sample complexity of learning the states. Besides their clear implications for the sample complexity of learning, our results also settle a long-standing open problem, namely that NOON states with  $N \geq 3$  photons cannot be generated deterministically by interfering an arbitrary product state, as they are not in the GE class. Earlier studies addressed only restricted cases involving number state inputs in linear optical settings<sup>18–20</sup>.

## Results

To characterize quantum correlations beyond HOM and boson sampling in bosonic systems, we introduce non-Gaussian-entangleable (NGE) states: these are the quantum states which cannot be generated via a generalized interference experiment (see Fig. 1), where separable quantum states are input to Gaussian protocols<sup>10,11</sup>. Conversely,

quantum states generated via generalized interference experiments are GE states. GE states are operationally meaningful, especially considering the recent progress of multi-mode quantum state engineering<sup>21,22</sup>. By definition, GE states include all Gaussian states and their convex mixtures<sup>23–28</sup>. In addition, they include states that are neither separable nor convex mixtures of Gaussian states, such as the output states of boson sampling experiments<sup>15</sup>, which involve identical photons scattering through a linear optical interferometer and whose measurement statistics is computationally hard to classically simulate. Moreover, the recently proposed multi-mode Gottesman–Kitaev–Preskill (GKP) states, with superior error correction performance over single-mode versions<sup>29–32</sup>, are GE—they can be engineered via applying Gaussian unitaries on single-mode GKP states<sup>31,32</sup>, reducing the challenge of multi-mode state engineering to preparing single-mode GKP states. On the contrary, NGE states will generally require a multi-mode non-Gaussian operation—or equivalently realized by Gaussian operations assisted with a sufficient amount of non-Gaussian ancilla<sup>33</sup>, creating a large overhead in quantum information processing.

To sharpen the distinction between GE and NGE states, we develop a convex resource theory<sup>34</sup> of genuine non-Gaussian entanglement. With GE states as the free states, the free operations are Gaussian protocols. Besides proving that NOON states with  $N \geq 3$  are NGE, we provide other examples of NGE states, such as superposition of two-mode squeezed vacuum states (TMSV). Furthermore, we introduce and analyze two monotones to quantify genuine non-Gaussian entanglement, one based on entanglement entropy (the *NG entanglement entropy*) and the other one based on the minimal number of ancillary modes necessary to convert an NGE state into a GE state (the *GE cost*). Moreover, we propose the GDE tomography protocol based on Gaussian unitary, local tomography (e.g., homodyne or heterodyne) and classical processing, and show its efficient learning in pure GE states and special classes of mixed GE states. We also establish a continuity proof for the robustness of our protocol for general states close to pure GE states. We show that the sample complexity of

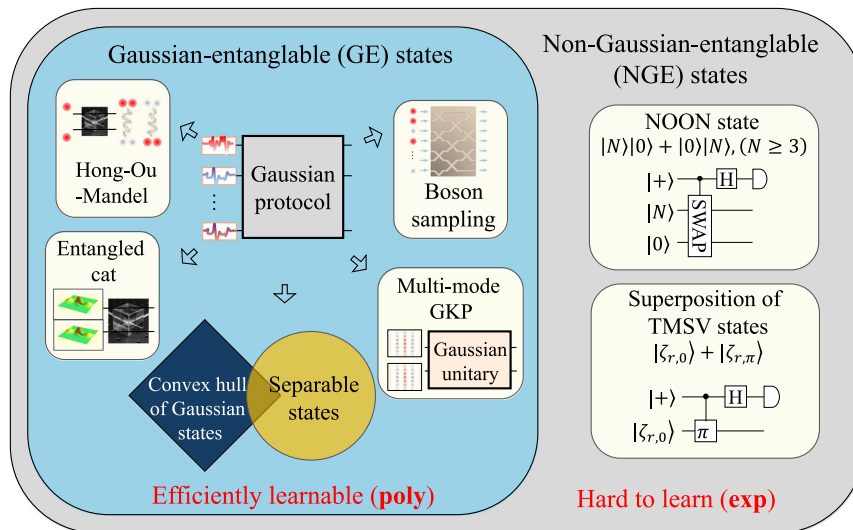


**Fig. 1 | Quantum correlations and the complexity of tomography.** Gaussian-entangleable (GE) state are states generated by performing Gaussian protocols on (possibly non-Gaussian) separable input states. The class of GE states includes the output state of the Hong–Ou–Mandel experiment, i.e., two photons input to a beam-splitter where photon bunching effect emerges, and the output states of the boson sampling protocol, where single photons together with vacuum states are input into a multi-mode linear interferometer. Other examples include entangled cat states, obtained by applying a beam-splitter to two identical cat states, and multi-mode GKP states, generated by performing Gaussian unitaries on single-

mode GKP states. In addition, the class of GE states encompasses both the convex hull of Gaussian states and the entire set of separable states. Here, we prove that the NOON state  $|N\rangle|0\rangle + |0\rangle|N\rangle$  with  $N \geq 3$ , superposition of TMSV states  $|\zeta_{r,0}\rangle + |\zeta_{r,\pi}\rangle$ , and the two-mode arithmetic progression state (see Supplemental Note 4) do not belong to the set of GE states. These states are conventionally generated by applying controlled gates followed by post-selection. At last, we show that the sample complexity in learning pure GE states scales as  $\sim \text{poly}(m)$  regarding number of modes  $m$ ; while NGE state generally requires an exponential overhead  $\sim \text{exp}(m)$ .

**Table 1 | Main results of this work**

Classification of quantum states	Main results	
GE states	Decomposition of pure GE states (Theorem 1)	Sample-efficient algorithm for learning GE states (Theorem 2, Theorem 3, and Corollary 4)
	Bounding the volume of GE state space (Corollary 10)	
NGE states	NOON states are NGE Supplemental Note 4	Exponential overhead in learning NGE states (Theorem 6 and Proposition 14)
	Establishment of resource monotones (Eqs. (7) and (8))	

tomography for pure GE states grows polynomially with the number of modes, while NGE states generally require an exponential overhead, quantified by their GE cost. This implies that output states in boson sampling experiments are easy to learn, despite their measurement statistics being hard to sample from with a classical computer<sup>15</sup>. We also provide numerical verification of the tomography process. The main results of this work are summarized in Table 1.

**Continuous-variable systems and state learning**

Continuous-variable quantum systems model continuous degrees of freedom, such as optical fields<sup>35</sup>, mechanical motions of ions<sup>36</sup>, and microwave cavities<sup>37</sup>. Owing to their information-rich infinite-dimensional Hilbert space, these systems are crucial for quantum communication<sup>38</sup>, quantum sensing<sup>39,40</sup>, quantum error correction<sup>22,33</sup>, and quantum computing<sup>41</sup> (see Supplemental Note 1A).

While general states of continuous-variable quantum systems are unbounded in energy, we are interested in practically relevant states with energy constraints. In particular, we consider  $m$ -mode quantum states with finite energy moment constraint,  $[\text{Tr} \hat{E}_m^k \hat{\rho}]^{1/k} \leq mE$ , where the energy operator  $\hat{E}_m = \frac{1}{4} \sum_{\ell=1}^m (\hat{q}_\ell^2 + \hat{p}_\ell^2)$  is a quadratic function of the position and momentum quadratures  $\hat{q}_\ell$  and  $\hat{p}_\ell$  in natural units  $\hbar = 2$ . We denote the set of  $m$ -mode pure states satisfying this  $k$ -th energy moment constraint as  $\mathcal{H}_{m,E}^k$ . We denote the set of mixed states satisfying the same energy constraint as  $\text{St}(\mathcal{H}_{m,E}^k)$ .

Learning a state within a trace distance error of  $\epsilon$  is equivalent to pinpointing it in state space within an  $\epsilon$ -ball with respect to the trace distance metric. The number of such  $\epsilon$ -balls—the volume—of the state space that the unknown state belongs to can manifest the challenge of state learning. It has been shown in ref. 7 that, for pure states subject to  $k$ -th moment constraint, the volume of the state space grows double-exponentially with the system size, scaling as  $\exp\left[\left(\frac{E}{12\epsilon^2 k}\right)^m\right]$ .

**Gaussian state and protocols**

Among bosonic states and operations, Gaussian states (e.g., coherent states and squeezed states), and operations (e.g., beam splitters, phase rotations, and squeezing) are not only analytically tractable but also experimentally friendly<sup>10,11</sup>.

Gaussian states are specific types of quantum states with their Wigner characteristic function in a Gaussian form<sup>42,43</sup>; therefore, a Gaussian state  $\hat{\rho}$  is uniquely specified by its mean  $\boldsymbol{\xi} := \text{Tr}[\hat{r}\hat{\rho}]$  and covariance matrix  $V := \frac{1}{2} \text{Tr}[\{(\hat{r} - \boldsymbol{\xi}), (\hat{r} - \boldsymbol{\xi})^\top\} \hat{\rho}]^{10,11}$ , where  $\hat{r} = [\hat{q}_1, \hat{p}_1, \dots, \hat{q}_m, \hat{p}_m]^\top$  is the vector of quadrature operators. For instance, the TMSV, defined as  $|\zeta_{r,\phi}\rangle_{AB} = (\cosh r)^{-1} \sum_{k=0}^\infty e^{ik\phi} (\tanh r)^k |k\rangle_A |k\rangle_B$ , have zero-mean and are uniquely determined by a covariance matrix that depends on the squeezing strength  $r$  and phase angle  $\phi$ . Here  $|k\rangle$  is the Fock state with photon number  $k$ . Gaussian quantum channels are completely positive trace-preserving maps that transform all Gaussian states into Gaussian states (see Supplemental Note 1B). In the following text, we shall use the notation  $\mathbb{G}(\mathcal{H})$  and  $\mathbb{GU}(\mathcal{H})$  to represent the set of all Gaussian quantum channels and unitaries on

the Hilbert space  $\mathcal{H}$ . More generally, a Gaussian protocol<sup>27</sup> includes the following set of quantum operations: (1) Gaussian unitaries on the system or part of the system, (2) partial trace, (3) composition with ancillary vacuum states, (4) probabilistically applying the above operations. Note that we exclude Gaussian measurements followed by the conditional operations (1)–(4) from the set of Gaussian protocols we consider, because these are more challenging from an experimental standpoint and the resulting feed-forward scheme might not reduce to a convex mixture of Gaussian channels.

Gaussian protocols (1)–(4) alone, without non-Gaussian ancilla, are limited in power—they are not universal for various tasks<sup>44–51</sup>. As it turns out, even when allowing for non-Gaussian input states, the generalized Gaussian interference process in Fig. 1 can only generate a limited class of states, as we define below.

**Gaussian-entangleable state**

Consider a bi-partition of the Hilbert space  $\mathcal{H} = \mathcal{H}_A \otimes \mathcal{H}_B$ . A quantum state  $\hat{\rho}_{AB}$  is (bi-partite) GE if it can be obtained by probabilistically applying a Gaussian protocol  $\mathfrak{G}_x$  on an ensemble of (possibly non-Gaussian) separable state  $\hat{\sigma}_{AB,y} \in \text{SEP}(\mathcal{H}_A \otimes \mathcal{H}_B)$  as  $\hat{\rho}_{AB} = \sum_{x',y} p_{x',y} \mathfrak{G}_{x'}(\hat{\sigma}_{AB,y})$  with  $p_{x',y}$  being a joint probability distribution. Equivalently, a GE state can be expressed as:

$$\hat{\rho}_{AB} = \sum_{x,y} p_{x,y} \mathcal{G}_x(\hat{\sigma}_{AB,y}), \tag{1}$$

where  $p_{x,y}$  refers to a joint probability distribution and  $\mathcal{G}_x \in \mathbb{G}(\mathcal{H}_A \otimes \mathcal{H}_B)$  denotes a Gaussian channel.

In practice, the GE state in Eq. (1) can be obtained by sampling from the joint probability distribution  $p_{x,y}$ , preparing the separable input state  $\hat{\sigma}_{AB,y}$ , and implementing the channel  $\mathcal{G}_x$ . When  $\mathcal{G}_x$  is unitary, it corresponds to randomly applying Gaussian unitaries on separable states. By definition, the set of GE states is convex—a mixture of GE states is still GE.

As schematically illustrated in Fig. 1, GE states can be non-Gaussian, and even not a convex mixture of Gaussian states. For instance, all entangled states generated by beam-splitter interference of non-Gaussian states, such as number states, are GE, e.g., the state  $(|0\rangle_A |2\rangle_B + |2\rangle_A |0\rangle_B) / \sqrt{2}$  from the HOM effect<sup>12</sup>. Similarly, the entangled cat state<sup>21</sup>  $\propto |\underline{\alpha}\rangle_A |\underline{\alpha}\rangle_B + |-\underline{\alpha}\rangle_A |-\underline{\alpha}\rangle_B$  is GE, as it can be generated using a balanced beam-splitter on a product of cat state and vacuum,  $\propto |\text{cat}\rangle_{\sqrt{2}\alpha,A} \otimes |0\rangle_B$ . Here  $|\underline{\alpha}\rangle$  is a coherent state with amplitude  $\alpha$ , and  $|\text{cat}\rangle_\alpha \propto |\underline{\alpha}\rangle + |-\underline{\alpha}\rangle$  denotes a cat state. (Here, we have introduced the underline to distinguish between coherent states and number states, omitted in the special case of the vacuum state  $|0\rangle$ .) Moreover, one can obtain a state  $\propto |\text{cat}\rangle_{\sqrt{2}\alpha,A} |0\rangle_B + |0\rangle_A |\text{cat}\rangle_{\sqrt{2}\alpha,B}$  via interference between two identical cat states  $|\text{cat}\rangle_\alpha$ . Other examples include GE states generated by the multi-mode GKP encoding process:  $|\psi\rangle_{m \rightarrow m+m'} = \hat{U}^{\text{GKP}}(|\psi\rangle_m \otimes |\text{GKP}\rangle^{\otimes m'})$ , where  $\hat{U}^{\text{GKP}}$  is a multi-mode Gaussian unitary,  $|\psi\rangle_m$  is an arbitrary  $m$ -mode state,  $|\text{GKP}\rangle$  is the canonical GKP state. Any multi-mode GKP state is also GE<sup>29–32</sup>.

As we show, one can obtain any pure GE states from Gaussian unitary on a product state, as shown below.

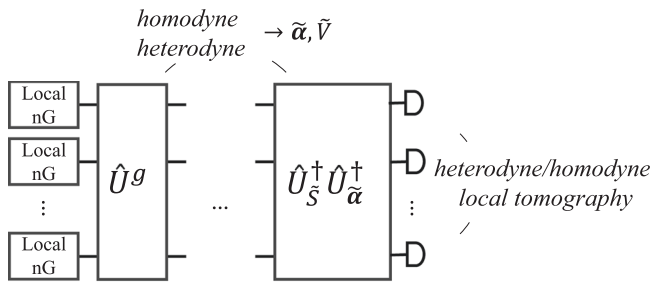


**Fig. 2 | The GDE tomography protocol simply using local state tomography.** First, we estimate the displacement  $\alpha$  and covariance matrix  $V$  by homodyne and heterodyne measurements. Based on the results, we subsequently apply a calibrated Gaussian unitary  $\hat{U}_s^\dagger \hat{U}_\alpha^\dagger$  to counter-rotate the state, and finally perform local tomography to reconstruct the local states. When the symplectic eigenvalues are non-degenerate, the Gaussian entangling unitary  $\hat{U}^g$  is fully identified and the counter-rotated states is separable; Otherwise, the state becomes passive-separable and we continue with the process depicted in Fig. 3.

**Theorem 1.** (Decomposition of pure GE states): Any pure GE state can be expressed in the following form:

$$|\psi\rangle_{AB} = \hat{U}^g |\phi\rangle_A |\phi'\rangle_B, \tag{2}$$

where  $\hat{U}^g$  is a Gaussian unitary,  $|\phi\rangle$  and  $|\phi'\rangle$  are local states of systems  $A$  and  $B$ .

The proof, as elaborated in Supplemental Note 2, is based on the concavity of entropy, Gaussian unitary decompositions, and more importantly the fact that the only states that remain pure under multi-mode pure loss are coherent states, which generalizes a single-mode result that is crucial for solving the minimum entropy output conjecture and the Gaussian state majorization conjecture<sup>52,53</sup> (see Lemma 7 in “Methods”).

GE states possess several distinctive properties (see details in Supplemental Note 3). For a pure Gaussian state with a non-degenerate symplectic spectrum, the condition that its covariance matrix is block-diagonal (linear uncorrelated) is equivalent to the state being a product state (independent). This equivalence fails when the symplectic eigenvalues are degenerate. In addition, Gaussian protocols map GE states to GE states. At last, one can extend the definition of bi-partite GE states in Eq. (1) and Theorem 1 to a multipartite  $m$ -mode case.

Furthermore, one can denote the covariance matrix of  $|\psi\rangle_{AB}$  as  $V_{AB}$ . For any symplectic matrix  $S$  such that  $SV_{AB}S^T = \Lambda$  is the Williamson diagonal form, the corresponding Gaussian unitary  $\hat{U}_S$  is equivalent to  $\hat{U}^g$  in Eq. (2) up to a beam-splitter  $\hat{U}_O$  for an orthogonal matrix  $O$  and a displacement operation  $\hat{D}^{10}$ , i.e.,  $\hat{U}^g = \hat{D} \hat{U}_S \hat{U}_O$ . If the symplectic eigenvalues of  $V_{AB}$  are non-degenerate, we have  $\hat{U}^g = \hat{D} \hat{U}_S (\hat{U}_A^g \otimes \hat{U}_B^g)$ , where  $\hat{U}_A^g \otimes \hat{U}_B^g$  is a tensor product of phase shifters. Hence, by first measuring the mean vector and covariance matrix, then applying the partial inverse  $\hat{U}_S^\dagger \hat{D}^\dagger$  of the Gaussian unitary, any GE state can be transformed into a passive-separable state (GE states with only passive beam-splitters as the entangling operation). The next section outlines a tomography protocol for GE states that exploits this counter-rotation step.

**Efficient learning of pure GE states**

As anticipated, pure GE states have reduced sample complexity for quantum state tomography, since one only needs to estimate the corresponding Gaussian unitary and local states by Theorem 1. In particular, we obtain the following result:

**Theorem 2.** (Sample complexity of pure GE states): Consider the set of  $m$ -mode pure states  $\{|\psi\rangle\}$  obtained by applying a Gaussian unitary to a

tensor product of single-mode states  $\{\otimes_{j=1}^m |\psi_j\rangle\}$ , where the states satisfy energy moment constraint,  $|\psi\rangle \in \mathcal{H}_{m,E}^2$ . Then, the tomography of such states requires  $M$  copies such that:

$$\Theta \left[ \frac{1 - \delta m E}{\log E} \frac{1}{\epsilon} \right] \leq M \leq \mathcal{O} \left[ \text{poly} \left( m, E, \frac{1}{\epsilon}, \log \frac{1}{\delta} \right) \right], \tag{3}$$

where  $\delta$  denotes the failure probability and  $\epsilon$  refers to the trace distance between the input and the reconstructed state.

The upper bound in Theorem 2 is demonstrated in Supplemental Note 7D, while the lower bound is determined by sample complexity of product states with moment constraints<sup>7</sup>. Therefore, the tomography of pure GE states is sample-efficient. For the case with a moderate number of modes in which constant prefactors in the sample complexity become important, we provide an explicit upper bound in Supplemental Note 7 F to offer more practical guidance for GE-state learning.

Below, we present the GDE learning protocol (see Fig. 2), involving a Gaussian unitary and then local state tomography. The local state tomography can be performed via different approaches, for example using heterodyne detection and classical processing. We begin with the simple example of passive separable states, where the physical Gaussian unitary is not needed. Then, we proceed to general pure GE states. In the next section, we generalize towards mixed GE states.

As a concrete example, consider the output state of an  $m$ -mode boson sampling process, known as passive-separable states  $\{|\psi_{ps}\rangle\}$ <sup>54</sup>, generated by applying a passive Gaussian unitary  $\hat{U}_O$  to a product state  $\{\otimes_{j=1}^n |\psi_j\rangle\}$ , where  $|\psi_j\rangle$  is a single-mode state (for multi-mode subsystem, we refer to Supplemental Note 7A). We present a tomography algorithm that takes as input  $M$  copies of the unknown state  $|\psi_{ps}\rangle = \hat{U}_O \otimes_{j=1}^n |\psi_j\rangle$ , output the classical description of a boson-sampling output state  $|\widetilde{\psi}_{ps}\rangle$  with smaller than  $\epsilon^2$  fidelity error with the input state  $|\psi_{ps}\rangle$  (leading to a trace distance error smaller than  $\epsilon$  by the Fuchs–van de Graaf inequality<sup>55</sup>) and a failure probability lower than  $\delta$ . As shown in Fig. 3, without relying on any adaptive strategy, the algorithm first performs heterodyne measurement on all  $M$  copies of the quantum states and then performs classical post-processing to obtain an estimate of the state.

To describe the post-processing algorithm, we denote the heterodyne measurement result  $q_k^{(\ell)} + ip_k^{(\ell)}$  for the  $k$ -th mode in the  $\ell$ -th copy. We collect all results as vectors  $\mathbf{y}^{(\ell)} = (q_1^{(\ell)}, p_1^{(\ell)}, \dots, q_m^{(\ell)}, p_m^{(\ell)})^T, 1 \leq \ell \leq M$ . Given the measurement results  $\mathbf{y}^{(\ell)}$ , the algorithm searches over all possible passive operations  $\hat{U}_O$  and goes over all possible local states  $|\psi_j\rangle$ . For each choice of  $\hat{U}_O$  and  $\{|\psi_j\rangle\}$ , we perform classical processing as detailed hereafter to obtain a fidelity lower bound estimate  $W$ . The exhaustive search ends when the fidelity lower bound estimate satisfies  $W \geq 1 - \epsilon^2$ , outputting the description of the corresponding estimate  $|\widetilde{\psi}_{ps}\rangle = \hat{U}_O \otimes_{j=1}^n |\psi_j\rangle$ . Otherwise, a failure is declared.

As sketched in Fig. 3, to obtain the fidelity lower bound estimate, we first calculate  $\alpha^{(\ell)} = O' \mathbf{y}^{(\ell)}$  and reconstruct all local states  $\{|\hat{\rho}_{j,O'}\rangle_{j=1}^m\}$ , whose matrix element in the number basis is

$$(\hat{\rho}_{j,O'})_{kk'} = \frac{1}{M} \sum_{\ell=1}^M \int_{\mathbb{C}^2} \frac{d^2 \mathbf{u}}{4\pi} e^{-|\mathbf{u}|^2} + \frac{i}{2} \left[ \frac{\alpha_{2j}^{(\ell)} \alpha_{2j+1}^{(\ell)}}{2} \right] \Omega \mathbf{u} \chi_{kk'}(\mathbf{u}), \tag{4}$$

where  $\Omega$  denotes the symplectic form (see “Methods”) and  $\chi_{kk'}(\mathbf{u})$  refers to the characteristic function of the operator  $|k\rangle\langle k'|$ . The above reconstruction is a standard heterodyne tomography<sup>56</sup>, but other reconstruction algorithms can also be adopted<sup>57,58</sup>. Finally, following

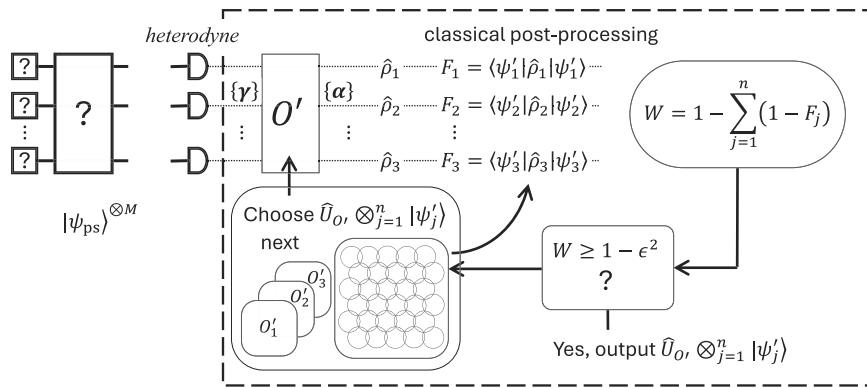


**Fig. 3 | Sample-efficient protocol for learning boson sampling output states.** It follows a non-adaptive procedure that uses only local measurement data: (i) Perform heterodyne measurement on all  $M$  state copies to collect phase-space samples  $\{\alpha\}$ . (ii) Iterate over an  $\epsilon$ -net of passive-separable states  $|\psi_{ps}\rangle = \hat{U}_O \otimes_{j=1}^n |\psi_j\rangle$ , reconstruct the corresponding local states  $\{\hat{\rho}_j\}$  after every passive operation  $\hat{U}_O$ , and evaluate a local fidelity  $F_j = \langle \psi'_j | \hat{\rho}_j | \psi'_j \rangle$  for each possible local state  $|\psi'_j\rangle$ . (iii) The first candidate with  $W := 1 - \sum_{j=1}^n (1 - F_j) \geq 1 - \epsilon^2$  is accepted as the reconstructed state; otherwise the protocol aborts.

reconstruct the corresponding local states  $\{\hat{\rho}_j\}$  after every passive operation  $\hat{U}_O$ , and evaluate a local fidelity  $F_j = \langle \psi'_j | \hat{\rho}_j | \psi'_j \rangle$  for each possible local state  $|\psi'_j\rangle$ . (iii) The first candidate with  $W := 1 - \sum_{j=1}^n (1 - F_j) \geq 1 - \epsilon^2$  is accepted as the reconstructed state; otherwise the protocol aborts.

ref. 59, we can compute the fidelity witness estimate

$$W = 1 - \sum_{j=1}^n (1 - F_j), \tag{5}$$

where each  $F_j = \langle \psi'_j | \hat{\rho}_j | \psi'_j \rangle$  is the local state fidelity for the current estimate.

A challenge in the classical processing is that it needs to go over all possible guesses of  $\hat{U}_O$  and local states, which are parameterized by continuous parameters with infinite possibilities. The way out of this dilemma is that we only require a finite error in the state learning: the finite-error relaxation allows one to establish a discrete set of  $\epsilon$ -balls of the possible  $\hat{U}_O$  and local states. Essentially, learning the parameters up to a discrete set of values suffices for meeting the  $\epsilon$  error requirement. Accordingly, for each of the  $\epsilon$ -balls, we take the mean values as the choice and perform a fidelity test, which also has a failure probability of not satisfying the needed error tolerance. The failure probability then builds up with the number of  $\epsilon$ -balls—generally a huge number. On the other hand, the failure probability decreases exponentially with the number of samples  $M$ ; therefore, the required number of samples is logarithmic of the number of  $\epsilon$ -balls. As a result, the key part of the proof of Theorem 2 is to upper bound the number of  $\epsilon$ -balls (the volume) required for boson-sampling states, as we analyze in the “Methods” section in detail.

With the sample-efficient learning of passive-separable states introduced, the generalization to arbitrary GE states can be obtained by applying a Gaussian unitary to reduce a GE state to a passive-separable state, hence, we name the protocol Gaussian-disentangling (GDE) learning. To do so, we first estimate the mean and covariance matrix of the input state to estimate a symplectic matrix  $S$  which diagonalizes the covariance matrix. Here, one can use either homodyne or heterodyne for covariance matrix estimation. Based on  $S$ , we apply a Gaussian unitary to reduce the input GE state to a zero-mean passive-separable state, which then can be sample-efficiently learned via the algorithm sketched in Fig. 3. The details can be found in Supplemental Note 7.

### Towards efficient learning of mixed GE states

In practice, preparing ideal pure GE states may be infeasible. Noise, loss, and decoherence can lead to mixed states, in which case the counter-rotation step may fail to map it to a passive separable form. Nevertheless, we find that some specific mixed GE states remain learnable via GDE tomography, with sample complexity polynomial in the number of modes.

First, we demonstrate that our GDE learning algorithm is *robust* against small perturbations caused by general (potentially

non-Gaussian) noise. Even if the unknown state is a slightly perturbed GE state—technically, a state constructed by sending an input state, which is  $\epsilon_{\text{input}}$ -close to a pure product state, into a channel, which is  $\epsilon_{\text{channel}}$ -close to a Gaussian unitary—our GDE learning algorithm remains effective and tomography remains efficient. In “Methods”, we show that the corresponding estimation errors for moments have fixed floors of order  $\mathcal{O}(\sqrt{\epsilon_{\text{channel}} + \epsilon_{\text{input}}})$  and  $\mathcal{O}(\epsilon_{\text{channel}}) + \mathcal{O}(\epsilon_{\text{input}}^{1/8})$  for the approximated passive-separable state after counter-rotation. If we assume that the input error  $\epsilon_{\text{input}}$  vanishes, we have the following theorem:

**Theorem 3.** Consider an approximated pure GE state  $\hat{\rho}$  acting on  $\mathcal{H}_{m,E}^2$  whose entangling channel is  $\epsilon_{\text{channel}}$ -close to an arbitrary Gaussian unitary. The sample complexity of learning this class of state is

$$M \simeq \mathcal{O}\left(\text{poly}\left(m, E, \frac{1}{\epsilon - \epsilon_{\text{channel}}}, \log\left(\frac{1}{\delta}\right)\right)\right), \tag{6}$$

for an error  $\epsilon > \epsilon_{\text{channel}}$  in trace distance and failure probability  $\delta$ .

The inequality  $\epsilon > \epsilon_{\text{channel}}$  arises because the measured state is known to be  $\epsilon_{\text{channel}}$ -close to the target, which induces an irreducible error floor for the estimators. A detailed discussion appears in Supplemental Note 8.

Second, we extend our discussion to GE states generated by applying a Gaussian unitary to a product of arbitrarily mixed states. In particular, this class includes the output of boson sampling under uniform photon loss and situations with detectors of equal efficiency. In the case where the symplectic eigenvalues of the input state has a finite eigengap  $\Delta$ , only moment estimation, Gaussian unitary, and local tomography will be used. Then, the following corollary holds:

**Corollary 4.** (Sample complexity of states entangled by a Gaussian unitary): Consider the set of  $m$ -mode states  $\{\hat{\rho}\}$  obtained by applying a Gaussian unitary to a tensor product of single-mode states  $\otimes_{j=1}^m \hat{\rho}_j$ , subject to an energy-moment constraint  $\hat{\rho} \in \text{St}(\mathcal{H}_{m,E}^2)$ . Meanwhile, the states’ symplectic eigenvalues are non-degenerate, up to a finite eigengap  $\Delta$ . The GDE protocol needs  $M \simeq \mathcal{O}(\text{poly}(m, E, \Delta^{-1}, \epsilon^{-1}, \log(\delta^{-1})))$  copies for this state family, for an error  $\epsilon$  in trace distance and failure probability  $\delta$ .

In Supplemental Note 8, we show that GDE protocol is able to achieve the sample complexity in Corollary 4, with local state tomography switched from fidelity witness in the pure-state case to heterodyne local tomography. The case of degenerate symplectic eigenvalues is not covered by the above Corollary. In Method, we show that there exist protocols relying on general measurements that

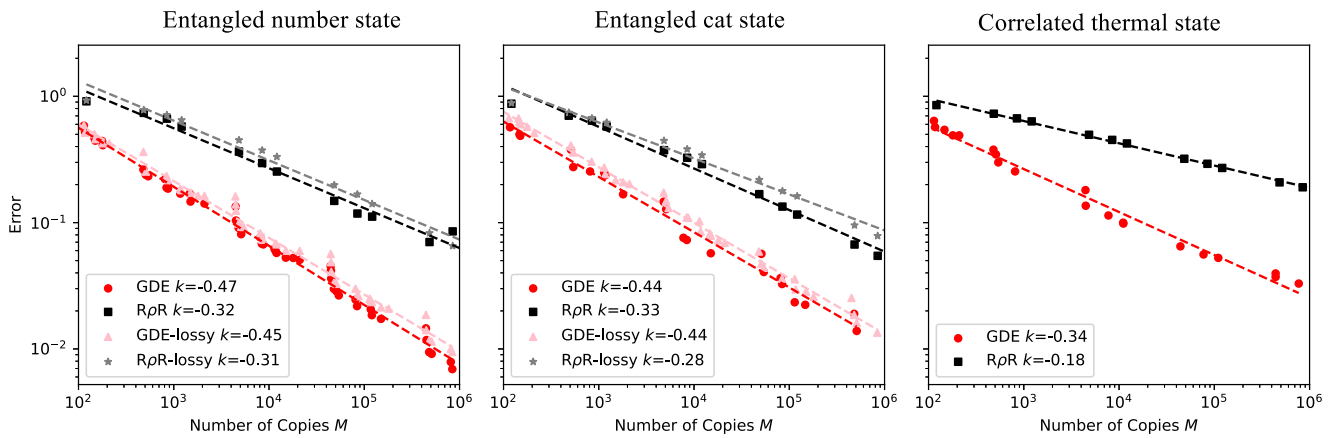


**Fig. 4 | Performance of Gaussian-disentangling protocol (GDE) versus direct tomography (RpR).** Here, we numerically simulate the quantum state tomography process on a two-mode GE state with the true state being number state  $|0\rangle \otimes |1\rangle$ , cat state  $|\text{cat}\rangle_{0,1} \otimes |\text{cat}\rangle_{1,1}$  and thermal state  $\rho_{\text{th},n=0.2} \otimes \rho_{\text{th},n=0.3}$  correlated by a beam-splitter (with a rotation angle  $\theta = \pi/4$ ). The error, defined as the trace distance between the true state and the reconstructed state obtained through direct tomography using the standard RpR algorithm<sup>2</sup>, is shown as a function of the number of copies  $M$  used in tomography (black squares for ideal case and grey stars

for the lossy case). In the lossy case, pure loss channel (with a transmissivity ratio  $\eta = 0.9$ ) is applied to both modes after the beam splitter. In contrast, the bottom envelope of achievable errors in the proposed Gaussian disentangling (GDE) algorithm, after minimising over possible sample number in estimating displacements and the covariance matrix, is given by red circles and pink triangles (lossy case). Their linear fit shows errors in GDE protocol decrease faster (with slope  $k$ ) compared to RpR method in all the three different states, demonstrating the advantage of GDE method.

in-principle guarantees sample-efficient learning of such degenerate states. Additionally, we provide a generalized GDE protocol with the hope of efficient learning such states with practical Gaussian operations, however, subject to an unproven conjecture.

Below, we apply Corollary 4 and Theorem 3 to practical experimental scenarios. In this regard, detector inefficiency is a ubiquitous and practically relevant imperfection that leads to mixed NGE states. Here, it can be modeled as ideal detection preceded by pure-loss channels. As uniform loss commutes with beam-splitters, it maps boson-sampling outputs to a passive Gaussian unitary acting on a product of mixed states. Consequently, Corollary 4 applies in the situation with non-degenerate symplectic eigenvalues, where both the sample and time complexity stay polynomial in the number of modes. For nonuniform loss, the degraded channel remains close to a Gaussian unitary in the low-loss regime. Thus, Lemma 11 in “Methods” guarantees a vanishing reconstruction error floor, and Theorem 3 shows that the sample complexity increases only polynomially with the degradation level.

To evaluate the performance of learning GE states, we numerically simulate the GDE tomography process for two-mode GE states with non-degenerate symplectic eigenvalues. As shown in Fig. 4, the GDE method, optimized over the copies allocated to estimating the mean vector and the covariance matrix (red and pink), achieves lower errors and markedly better scaling than direct tomography (black and gray)<sup>2</sup>. Details of the simulation are presented in Supplemental Note 7B.

### Non-Gaussian-entangleable states

While we have shown that GE states are efficiently learnable, we know that general quantum states are hard to learn<sup>7</sup>. This immediately indicates the existence of states that do not belong to the GE class defined in Eq. (1), which we refer to as NGE states. By definition, these states feature genuine non-Gaussian entanglement, which cannot be produced by Gaussian protocols. In practice, we show that NGE states can be produced by a multi-mode non-Gaussian unitary, or by a local non-Gaussian unitary acting on a non-trivial GE state. Furthermore, entanglement-breaking channels<sup>60</sup>, followed by Gaussian protocols, can destroy genuine non-Gaussian entanglement. Moreover, it can be quickly verified that a Gaussian unitary maps NGE states to NGE states (see Supplemental Note 3C).

From Theorem 1, we have an efficient protocol to identify pure NGE states (see “Methods”). As a result, we provide a few examples of NGE states (see Fig. 1), whose membership proofs can be found in Supplemental Note 4. Firstly, we prove that the NOON states  $|\text{NOON}\rangle \propto |N\rangle_A |0\rangle_B + |0\rangle_A |N\rangle_B$  are NGE for  $N > 2$ . This means that, aside from the trivial  $N = 1$  case, the  $N = 2$  case from the HOM effect is the only nontrivial instance of a beam-splitter generating NOON state—those with  $N > 2$  cannot be generated deterministically by any Gaussian protocol acting on two-mode separable states, including linear optical operations. Note that, for this specific problem, previous approaches have only established such a no-go result for number state inputs in a linear optical setting<sup>18–20</sup>, where the photon number is preserved and therefore it suffices to disprove the case with two-mode Fock state. Our approach completes the general case by reducing general Gaussian unitaries to passive unitaries.

In addition, we show that the superposition of a TMSV state and a  $\pi$ -phase rotated TMSV state,  $|\Psi_{\text{TMSV}}\rangle \propto |\zeta_{r,0}\rangle + |\zeta_{r,\pi}\rangle$  with  $r > 0$ , is also NGE. Such states are along the line of recent single-mode experiments generating non-classical superposition of Gaussian states in quantum systems with universal control<sup>61</sup>.

### Resource measures of genuine non-Gaussian entanglement

To quantify genuine non-Gaussian entanglement, we further employ the quantum resource theory framework<sup>34</sup>, which has been successful in quantifying quantum entanglement, quantum coherence and quantum non-Gaussianity. Here, we model all GE states as free states. To be general and also to provide insight into multi-mode state learning, we consider the case of multi-partite GE states, with  $n$  partitions  $\mathbf{A} = \{A_1, \dots, A_n\}$ , and define the Hilbert space  $\mathcal{H}_{\mathbf{A}}$  accordingly. On this account, Gaussian protocols are free operations as they map free states to free states (see Supplemental Note 3C). However, due to the multipartite nature of entanglement, the general quantification of genuine non-Gaussian entanglement faces similar challenges to the case of multipartite entanglement<sup>62</sup>.

To tackle this issue, we define the non-Gaussian entanglement entropy, abbreviated simply as the NG entropy (see Supplemental Note 5). Given an arbitrary  $n$ -partite pure state  $|\psi\rangle_{\mathbf{A}} \in \mathcal{H}_{\mathbf{A}}$ , denote  $\hat{\rho}_{\mathbf{A}}(\hat{U}^{\mathbf{G}}) = \hat{U}^{\mathbf{G}} |\psi\rangle_{\mathbf{A}} \langle\psi|_{\mathbf{A}} \hat{U}^{\mathbf{G}\dagger}$  and its reduced state as  $\hat{\rho}_{A_j}(\hat{U}^{\mathbf{G}}) = \text{Tr}_{k \neq j}[\hat{\rho}_{\mathbf{A}}(\hat{U}^{\mathbf{G}})]$ ;

the NG entropy is defined as:

$$\mathcal{E}_{\text{NG}}(|\psi\rangle\langle\psi|_{\mathcal{A}}) \equiv \min_{\hat{U} \in \text{GU}(\mathcal{H}_{\mathcal{A}})} \frac{1}{n} \sum_{j=1}^n H(\hat{\rho}_{A_j}(\hat{U}^{\otimes j})), \quad (7)$$

with  $H(\hat{\rho}) = -\text{Tr}[\hat{\rho} \log_2 \hat{\rho}]$  being the von Neumann entropy of the state  $\hat{\rho}$ . Here, we minimize over all Gaussian unitaries. Given an arbitrary pure GE state  $|\psi\rangle$ , the resource measure  $\mathcal{E}_{\text{NG}}$  satisfies the following criteria: (1)  $\mathcal{E}_{\text{NG}}(|\psi\rangle\langle\psi|) = 0$  if and only if  $\psi$  is GE; (2)  $\mathcal{E}_{\text{NG}}(|\psi\rangle\langle\psi|)$  is invariant under Gaussian unitaries. A numerical evaluation of the NG entropy for pure NGE states is shown in Fig. 5. For operational purposes, we may also define a measure as the maximum overlap between a given pure state and an arbitrary pure GE state (see “Methods”). This measure distinctly separates GE and NGE states: it is zero for every pure GE state and non-zero for any NGE state, and invariant under Gaussian unitaries.

As no single “golden unit” of multipartite entanglement exists due to the complex structure of multi-partite entanglement, we further introduce a vector resource measure to characterize multipartite genuine non-Gaussian entanglement. This resource measure is based on the number of ancillary modes necessary to make an NGE state GE: the GE cost defined below. To get a clearer picture, let us begin with a

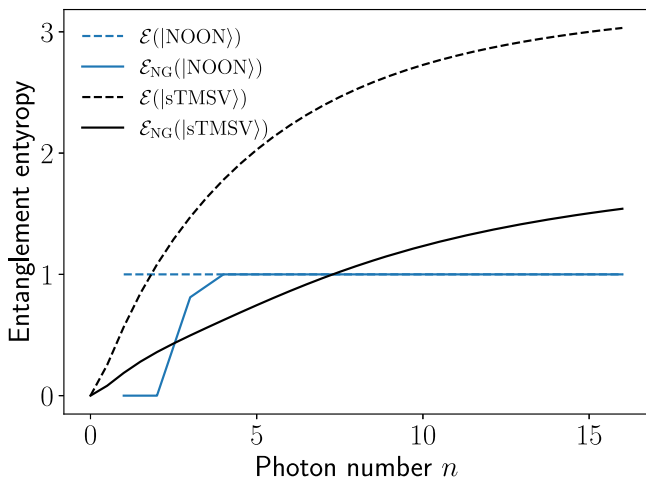


**Fig. 5 | Comparison between NG entropy and entanglement entropy.** The x-axis denotes the photon number, dashed lines indicate the entanglement entropy of the NOON state  $|\text{NOON}\rangle$  and a superposition of two TMSV states  $|\text{sTMSV}\rangle$ , while the solid lines reflect their NG entropy.

simple bi-partite system of two modes  $A$  and  $B$ . As shown in Fig. 6a, any NGE state  $\hat{\rho}_{AB}$  can be extended into a tri-partite state  $\hat{\rho}_{AB} \otimes \hat{\sigma}_C$  by introducing an ancilla  $C$ . Meanwhile, this state is naturally a GE state between  $AC$  and  $B$  because it can be generated from a separable state  $\hat{\rho}_{AC} \otimes \hat{\sigma}_B$  between  $AC$  and  $B$  via a fully transmissive beam-splitter, i.e., a Gaussian unitary operation swapping systems  $B$  and  $C$ . Likewise, for  $m$  single-mode subsystems, any NGE state can be produced by introducing an  $(m-1)$ -mode non-Gaussian ancillary state entangled with the first mode.

For simplicity of analysis, let us consider an  $n$ -mode state with  $n$ -partition, while the more general case can be found in Supplemental Note 6. The GE states are those generated by applying  $n$ -mode Gaussian protocols on a  $n$ -mode fully separable state. Then, the corresponding GE cost is given as follows:

**Definition 5.** (GE cost vector and GE cost function): Given an arbitrary  $n$ -mode density matrix  $\rho$  over  $\mathcal{H}_{\mathcal{A}}$ , a GE cost vector is defined as a list of ancillary-mode numbers in a decreasing order:

$$\mathcal{R}(\rho) = \{|A'_1|, \dots, |A'_n|\}, \quad (|A'_1| \geq |A'_2| \geq \dots \geq |A'_n|), \quad (8)$$

of an extension  $\rho_{\text{ext}}$  satisfying  $\rho = \text{Tr}_{A'_1, \dots, A'_n}[\rho_{\text{ext}}]$ , such that  $\rho_{\text{ext}}$  is a GE state that can be obtained by applying a Gaussian protocol on a separable state between  $A_1A'_1, A_2A'_2, \dots$  and  $A_nA'_n$ . We will denote the  $k$ -th entry of  $\mathcal{R}$  as  $\mathcal{R}_k$  and the number of nonzero entries of  $\mathcal{R}$  as  $\ell$ .

The GE cost function is then defined as:

$$\mathcal{R}_f(\rho) = \min_{\rho_{\text{ext}}} \mathcal{R}_1 \quad (9)$$

where the minimization is taken over all possible GE extensions  $\rho_{\text{ext}}$  of the original state  $\rho$ .

Figure 6b shows an example of six modes, where ancilla modes  $A'_1$  and  $A'_3$  are introduced to extend the state to a GE state. The definition of a GE cost vector is closely related to the concept of Young diagram, as it is connected to irreducible representations of the permutation group. Note that although we have introduced the extension procedure with swap operations, general Gaussian protocols can be applied.

Note that the GE cost vector is not unique, but the GE cost function is. Moreover, the GE cost function  $\mathcal{R}_f$  (as well as the one-norm of the GE cost vector  $\|\mathcal{R}\|_1 = \min_{\rho_{\text{ext}}} \sum_{j=1}^{\ell} \mathcal{R}_j$ ) are non-increasing under Gaussian protocols. In addition, the GE cost function  $\mathcal{R}_f$  can also be bounded as  $\|\mathcal{R}\|_1/\ell \leq \mathcal{R}_f \leq \|\mathcal{R}\|_1$ . In the next section, we will show that the GE cost function provides useful prior information for learning, as it guides how resources must be allocated in a tomography protocol.

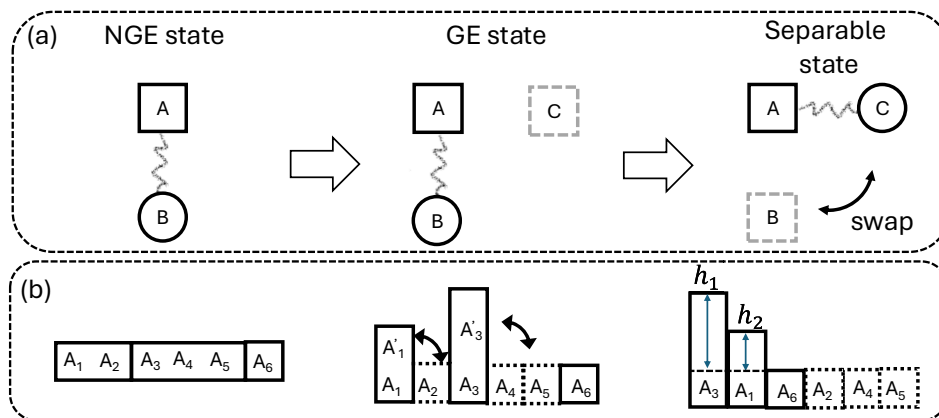


**Fig. 6 | Schematic of the state extension process.** **a** A bi-partite NGE state  $\hat{\rho}_{AB}$  can be extended to a tri-partite GE state  $\hat{\rho}_{AB} \otimes \hat{\sigma}_C$ . **b** Young diagram representation of a multipartite case of six modes. The states of subsystems  $A_1A_2$  and  $A_3A_4A_5$  are both

NGE. By introducing the ancilla  $A'_1$  and  $A'_3$ , the state is GE between  $A_1A'_1, A_2, A_3A'_3, A_4, A_5$  and  $A_6$ . In addition, we can permute local systems to have a sorted column length and  $\mathcal{R}(\psi) = (h_1, h_2, 0, 0, 0, 0)$ .

### Learning pure NGE states

The GE cost is operationally meaningful, as it directly connects to the generation procedure of an NGE state. Moreover, as the clear structure of entanglement indicates, the cost of learning NGE states can be quantified by the GE cost, as we show in the following. In particular, to leverage the Gaussian entangling procedure in defining the GE cost, we consider a learning algorithm based on the one for GE states, with the local states corresponding to the minimal subsystems of modes  $\{\mathcal{R}_k + 1\}$  that cannot be further disentangled by any Gaussian unitary (see details on “generalized GE states” in Supplemental Note 7).

When the number of modes  $m$  is large, the sample complexity is shown in Proposition 14 in “Methods”, which is an exponential function of  $\max_k \mathcal{R}_k$ . It is worth noting that, for any family of states, the GE cost plays the role of prior information that guides the choice between two strategies: (i) applying a counter-rotation followed by local tomography, or (ii) performing direct tomography on larger subspaces. The magnitude of the GE cost directly influences which strategy is preferable and, in turn, sets the overall sample complexity.

In general, one can have a tight scaling with respect to the GE cost for the non-degenerate scenario:

**Theorem 6.** (Sample complexity for non-degenerate case): Consider an energy-constrained  $m$ -mode pure state in  $\mathcal{H}_{m,E}^2$ , whose GE cost is specified by an  $l$ -element vector  $\mathcal{R}$  and the function  $\mathcal{R}_f$ . Meanwhile, its covariance matrix has non-degenerate symplectic eigenvalues with an eigengap  $\Delta$ . The required sample complexity for tomography is:

$$M = \text{poly}\left(\ell, E, \frac{1}{\Delta}, \frac{1}{\epsilon}, \log \frac{1}{\delta}\right) \cdot \Theta\left[\left(\frac{E}{\epsilon}\right)^{\mathcal{R}_f}\right] \quad (10)$$

where  $\text{poly}(\ell, E, \frac{1}{\epsilon}, \log \frac{1}{\delta})$  refers to a polynomial function of  $\ell, E$ , the error  $\epsilon$  in trace distance, and failure probability.  $\Theta$  denotes the big theta notation.

A detailed proof of Theorem 6 can be found in Supplemental Note 7E. In particular, we prove that the exponent of  $E/\epsilon$  in the upper bound achieved by our protocol matches that of the lower bound demonstrated in Proposition 14. However, a residual gap remains, scaling as  $\ell^{2\mathcal{R}_f}$ . Notably, the GE cost can be connected with the recently proposed  $t$ -doped bosonic Gaussian states<sup>7</sup>—states generated from unlimited multi-mode Gaussian unitaries and  $t\kappa$ -local non-Gaussian unitaries. Our results extend this class to the NGE class measured by the GE cost, and the tomography overhead is directly related to the GE cost. In particular, any  $t$ -doped state can be extended into a GE state with  $(\kappa t - 1)$  ancillary modes. From Theorem 6, the sample complexity of learning a GE state has an overhead  $\epsilon^{-\kappa t - 2}$  as its GE cost vector is  $\mathcal{R} = (\kappa t - 1, 0, \dots)$ .

### Discussion

In this work, we have identified a quantitative relationship between the nature of quantum correlations in bosonic systems and the complexity of quantum tomography, uncovering the role of genuine non-Gaussian entanglement—entanglement which cannot be produced by Gaussian protocols.

We point out a few open problems. We have focused on pure states in the study of sample complexity in learning, while deferring the generalization to mixed state to future work. There, the disentangling procedure for Gaussian multi-mode channels is to be developed. Another open question is the quantification of the genuine non-Gaussian entanglement for measurement, which represents a dual problem within the resource theory of NGE states. In addition, an intriguing open question is how to design a tomography protocol whose time complexity—specifically, the number of search rounds required within each  $\epsilon$ -covering net—scales polynomially with the number of modes, while preserving the already efficient sample

complexity. Finally, asymptotic conversion rate between NGE states and generalization to fermionic systems are also of interest.

### Method

#### Preliminary

An  $m$ -mode bosonic quantum system is completely specified by the statistical moments of its canonical quadrature operator vector  $\hat{r} = [\hat{q}_1, \hat{p}_1, \dots, \hat{q}_m, \hat{p}_m]^T$ . Its first and second moments are captured by the mean vector  $\xi := \text{Tr}[\hat{r}\hat{\rho}]$  and the covariance matrix  $V := \frac{1}{2} \text{Tr}[\{(\hat{r} - \xi), (\hat{r} - \xi)^T\}\hat{\rho}]^{10,11}$ . The first-moment changes are modeled by the displacement operation  $\hat{D}_\xi = \exp(-i\xi^T \Omega \hat{r})$ , where  $\xi = (\xi_1, \dots, \xi_{2m})$  denotes the vector of displacements and  $\Omega = \bigoplus_{j=1}^m \begin{pmatrix} 0 & 1 \\ -1 & 0 \end{pmatrix}$  refers to the symplectic form. Then, given an arbitrary operator  $\hat{X}$ , one can define the Wigner characteristic function  $\chi_{\hat{X}}(\xi) = \text{Tr}[\hat{X}\hat{D}_\xi]$ . For notational simplicity, we will let  $\chi_{kl}(\xi)$  denote the characteristic function of the operator  $|k\rangle\langle l|$ , where  $\{|k\rangle, k = 0, \dots, \infty\}$  is the Fock basis.

#### A useful lemma for the proof of Theorem 1

The proof of Theorem 1 is based on the following lemma:

**Lemma 7.** (Generalizing Lemma 2 in ref. 52): The only states that remain pure under multi-mode pure loss are coherent states.

The detailed proof of this lemma is given in Supplemental Note 2.

#### Verification of NGE states

From Theorem 1, we have the following corollary for the identification of NGE states:

**Corollary 8.** (Verification of pure NGE states): Let  $|\psi\rangle_{AB}$  be a bi-partite pure state and let  $S$  be a symplectic matrix that diagonalizes its covariance matrix, and  $\hat{U}_S^\xi$  be the corresponding Gaussian unitary. (1) If the symplectic eigenvalues are non-degenerate, and  $\hat{U}_S^\xi |\psi\rangle_{AB}$  is not a product state, then  $|\psi\rangle_{AB}$  is NGE. (2) If there is no beam-splitter network  $\hat{U}_O^\xi$  with orthogonal  $O$  such that  $\hat{U}_O^\xi \hat{U}_S^\xi |\psi\rangle_{AB}$  is a product state, then  $|\psi\rangle_{AB}$  is NGE.

#### Maximal fidelity in state preparation

Consider a specific partition of the Hilbert space  $\mathcal{H}_A = \bigotimes_{j=1}^n \mathcal{H}_{A_j}$ . Then, the maximal fidelity of preparing a pure state  $|\psi\rangle_A \in \mathcal{H}_A$  from any GE state  $|\psi'\rangle_A \in \mathcal{H}_A$  can be obtained as follows:

$$\mathcal{P}_{\text{NG}}(|\psi\rangle\langle\psi|_A) = \max_{\substack{|\phi\rangle_j \in \mathcal{H}_{A_j} \\ \forall j=1, \dots, n \\ \hat{U}^\xi \in \text{GU}(\mathcal{H}_A)}} \left| \langle \psi|_A \hat{U}^\xi \bigotimes_{j=1}^n |\phi\rangle_j \right|^2 \quad (11)$$

$$\equiv \max_{\hat{U}^\xi \in \text{GU}(\mathcal{H}_A)} \left\| \hat{U}^{\xi^\dagger} |\psi\rangle\langle\psi|_A \hat{U}^\xi \right\|_x, \quad (12)$$

where  $\|\cdot\|_x = \max_{\phi_j \in \mathcal{H}_{A_j}} \bigotimes_{j=1}^n \langle \phi_j| \cdot \bigotimes_{k=1}^n |\phi_k\rangle$  refers to the cross norm. Note that the cross norm can be bounded by the operator norm as  $\|\hat{X}\|_x \leq \|\hat{X}^{\dagger A_0}\|_\infty$ , ( $A_0 \subset A$ ), which can be computed efficiently.

#### Volume of the state space

A crucial step in the proofs of Theorem 2 and Proposition 14 is to show that Algorithm 2 in Supplemental Note 7A requires fidelity-witnesses on  $\exp(\mathcal{O}[\text{poly}(m)])$  passive-separable states, so that applying the union bound<sup>56</sup> yields a polynomial sample complexity (see Supplemental Note 7C, D).

Intuitively, given that the state is known to lie within a specific class, the problem of determining how many states can be

distinguished by tomography reduces to quantifying the amount of classical information required to specify any state in that class to within an error  $\epsilon$ . The associated quantity can also be referred to as the state description complexity or volume of the state space, whose logarithm determines the number of classical bits required to transmit the information. More rigorously, the following definition is given:

**Definition 9.** ( $\epsilon$ -covering net): Let  $\mathcal{S}$  denote a set of  $m$ -mode pure states. Then, there exists a  $\epsilon$ -covering net  $\mathcal{S}_{\text{net}} \subset \mathcal{S}$ , such that for every  $|\psi\rangle \in \mathcal{S}$ , there exists  $|\psi'\rangle \in \mathcal{S}_{\text{net}}$  satisfying  $\|\ |\psi\rangle\langle\psi| - |\psi'\rangle\langle\psi'| \|_1 / 2 \leq \epsilon$  where  $\|X\|_1 = \sqrt{\text{Tr}[X^\dagger X]}$  denotes the trace norm.

Thus, the number of target states that require certification in tomography—referred to as the ‘volume’ of the state space—is determined by the cardinality of the corresponding  $\epsilon$ -covering net. To visualize the upper bound, let us look at a more general case with GE states:

**Corollary 10.** (Volume of GE state space): Consider the set of  $m$ -mode pure GE states  $\{|\psi\rangle \in \mathcal{H}_{m,E}^1\}$  produced by applying a Gaussian unitary on the tensor product of single-mode states. The size of the corresponding  $\epsilon$ -covering net is bounded by:

$$|\mathcal{S}_{\text{ge,net}}| \leq \exp\left(\mathcal{O}\left[\text{poly}\left(m^3, E, \frac{1}{\epsilon^2}\right)\right]\right). \tag{13}$$

The proof of Corollary 10 is shown in Supplemental Note 7. In contrast, the size of  $\epsilon$ -covering net for all pure states in  $\mathcal{H}_{m,E}^1$  is lower bounded as  $|\mathcal{S}_{\text{e,net}}| \geq \exp\left(\Theta\left[\left(\frac{E}{12\epsilon^2}\right)^m\right]\right)^7$ .

In our algorithm, we propose local fidelity witnesses to approximate the global fidelity witness for passive-separable states (see Fig. 3). This requires slightly fewer observables than the ‘‘volume’’ of passive-separable states, which is already smaller than that of GE states in Eq. (13)—at the cost of a controllable global fidelity witness error (see Supplemental Note 7A for details).

In our discussion of mixed-state learning, we use an  $\epsilon_2$ -covering net of symplectic orthogonal matrices. Formally, let

$$\mathcal{S}_{\text{net},\mathcal{O}} \subseteq \text{U}(m) \tag{14}$$

be a set of  $2 \times 2m$  symplectic orthogonal matrices such that, for every symplectic orthogonal matrix  $O$ , there exists  $O' \in \mathcal{S}_{\text{net},\mathcal{O}}$  with  $|O_{jk} - O'_{jk}| \leq \epsilon_2 \ \forall j, k \in \{1, \dots, 2m\}$ , where  $\{O_{jk}\}$  denotes the matrix elements of  $O$ .

**A useful lemma for mixed GE-state learning**

In the main text, we mention a continuity proof for the learning protocol for pure GE states. Although the details are presented in Supplemental Note 8 B, we present a crucial lemma here that may be of interest by itself.

First, the state of interest can be defined as follows:

$$\hat{\rho}_{\text{mix}} = \mathcal{C}_A \left( \bigotimes_{j=1}^m \hat{\rho}_j \right) \left\{ \begin{array}{l} \frac{1}{2} \min_{\mathcal{U}_A^g \in \text{GU}(\mathcal{H}_A)} \| \mathcal{C}_A - \mathcal{U}_A^g \|_{\diamond}^{E,2} \leq \epsilon_{\text{channel}} \\ \frac{1}{2} \left\| \bigotimes_{j=1}^m \hat{\rho}_j - \bigotimes_{j=1}^m |\psi_j\rangle\langle\psi_j| \right\|_1 \leq \epsilon_{\text{input}} \end{array} \right. , \tag{15}$$

where  $\mathcal{C}_A$  is an arbitrary  $m$ -mode quantum channel acting on the sub-systems  $\{A_1, \dots, A_m\}$ ,  $\mathcal{U}_A^g(\cdot) = \hat{U}^g \cdot \hat{U}^{g\dagger}$  refers to an arbitrary Gaussian unitary channel,  $\| \mathcal{C}_A \|_{\diamond}^{E,2} = \sup_{\substack{|\Psi_{AB}\rangle \\ \text{Tr}_{\mathcal{B}}[|\Psi\rangle\langle\Psi|_{AB}] \in \text{St}(\mathcal{H}_{m,E}^2)}}$   $\| (\mathcal{C}_A \otimes I_B)(|\Psi_{AB}\rangle\langle\Psi_{AB}|) \|_1$  is the diamond norm with bounded second moment of input energy,  $\hat{\psi}_{\text{pure}} = \hat{U}^g(\bigotimes_{j=1}^m |\psi_j\rangle\langle\psi_j|)\hat{U}^{g\dagger}$  is the ideal state, and we have

$\hat{\rho}_{\text{mix}}, \hat{\psi}_{\text{pure}}, \bigotimes_{j=1}^m \hat{\rho}_j, \bigotimes_{j=1}^m |\psi_j\rangle\langle\psi_j| \in \text{St}(\mathcal{H}_{m,E}^2)$ . In the following, we denote  $\epsilon_{\text{mix}} = \epsilon_{\text{channel}} + \epsilon_{\text{input}}$  as the total error.

Then, we have a lemma concerning all errors.

**Lemma 11.** Let  $\hat{\rho}_{\text{mix}}$  be an approximate GE state described by Eq. (15). The estimation errors of the GDE protocol, designed for pure states, obey

$$\epsilon \leq f\left(\|\xi - \tilde{\xi}\|_2, \|V_{\text{pure}} - \tilde{V}\|_{\infty}^{1/4}\right) + \epsilon'_{\text{ps}}, \tag{16}$$

$$\|\xi - \tilde{\xi}\|_2 \leq 8\sqrt{E\epsilon_{\text{mix}}} + \frac{\epsilon_v}{20\sqrt{mE}}, \tag{17}$$

$$\|V - \tilde{V}\|_{\infty} \leq 40\sqrt{2E}\sqrt{\epsilon_{\text{mix}}} + \epsilon_v, \tag{18}$$

$$\epsilon'_{\text{ps}} \leq \epsilon_{\text{channel}} + f\left(\|\xi - \tilde{\xi}\|_2, \|V_{\text{pure}} - \tilde{V}\|_{\infty}^{1/4}\right) + \epsilon_{\text{ps}}, \tag{19}$$

where  $\epsilon$  denotes the reconstruction error in tomography,  $\xi$  and  $V_{\text{pure}}$  denote the displacement and covariance matrix of the state  $\psi_{\text{pure}}$ ,  $f(\|\xi - \tilde{\xi}\|_2, \|V_{\text{pure}} - \tilde{V}\|_{\infty}^{1/4}) = \mathcal{O}(\|\xi - \tilde{\xi}\|_2) + \mathcal{O}(\|V_{\text{pure}} - \tilde{V}\|_{\infty}^{1/4})$  is the error of estimating moments, the first terms in Eqs. (17)–(19) constitute a fixed error floor, the second terms of Eqs. (17) and (18) give the errors for an ideal pure input,  $\epsilon'_{\text{ps}}$  is the error of estimating the approximated passive separable state after counter-rotation based on estimating moments,  $\epsilon_{\text{ps}}$  denotes the corresponding error where we have an ideal pure GE state.

In this regard, the GDE learning protocol remains robust provided that the approximation errors  $\epsilon_{\text{channel}}$  and  $\epsilon_{\text{input}}$  vanish. When the input error  $\epsilon_{\text{input}}$  vanishes, we have Theorem 3 in the main text. A detailed derivation of Lemma 11 is shown in Supplemental Note 8.

**Learning degenerate mixed GE states**

To go beyond Corollary 4 which only addresses the non-degenerate case, we begin with a complexity upper bound that guarantee efficiency, achieved by general joint measurements.

**Theorem 12.** (Application of Theorem 1.5 in ref. 63): Consider the set of  $m$ -mode states  $\{\hat{\rho}\}$  obtained by applying a Gaussian unitary to a tensor product of single-mode states  $\bigotimes_{j=1}^m \hat{\rho}_j$ , subject to an energy-moment constraint  $\hat{\rho} \in \text{St}(\mathcal{H}_{m,E}^2)$ . There exists a tomography algorithm for this class of states that achieves the sample complexity  $M = \mathcal{O}(\text{poly}(m, E_{\text{II}}, \frac{1}{\epsilon}, \log(\frac{1}{\delta})))$ .

A concrete proof of Theorem 12 is shown in Supplemental Note 8. In general, Theorem 12 implies the existence of an efficient learning algorithm for mixed Gaussian-unitary-entangleable states, possibly using non-Gaussian joint measurements. Whether homodyne or heterodyne measurements with classical postprocessing suffice remains open and is left to future work.

In this regard, we propose in Supplemental Note 8 a generalized-GDE tomography protocol for arbitrary mixed states entangled by a Gaussian unitary. The protocol reduces back to the GDE protocol for the non-degenerate case (and thus efficient); for the degenerate case, the protocol is efficient up to an unproven conjecture. In the following, we briefly summarize the generalized GDE protocol.

The first few steps of generalized-GDE are identical to the GDE protocol, where we estimate the covariance matrix and then perform the disentangling Gaussian unitary. When the symplectic eigenvalues are non-degenerate, we would conclude with the local tomography as in Corollary 4. If the symplectic eigenvalues are degenerate, then we continue with the next step of generalized-GDE. We classically build an  $\epsilon$ -covering net of all  $2m \times 2m$  symplectic orthogonal matrices, so that for any  $O$  there exists  $O'$  in the net with entrywise deviation at most  $\epsilon_2$ .

For each  $O'$  in the net  $\mathcal{S}_{\text{net},O'}$ , we reconstruct  $\tilde{\rho}_{\text{ps},O'} = \hat{U}_{O'} \left[ \otimes_{j=1}^m \hat{\rho}_{j,O'} \right] \hat{U}_{O'}^\dagger$ , where  $\hat{\rho}_{j,O'}$  is the reconstructed reduced state from heterodyne measurement in Eq. (4). To precisely obtain all of these reconstructed states, we can build up  $L \propto m(1/\epsilon_2)^{4m^2}$  local observables and rely on shadow tomography<sup>56</sup> to estimate them from heterodyne data on  $\mathcal{O}(\log L) \sim \mathcal{O}(\text{poly}(m))$  copies.

For each of the  $\tilde{\rho}_{\text{ps},O'}$ , we perform a reduced-state test, which is the replacement of fidelity witness that only works for pure states. In this test, we apply virtual passive rotations  $\hat{U}_{O_f}^\dagger$  classically, compute reduced states of  $\hat{U}_{O_f}^\dagger \tilde{\rho}_{\text{ps},O'} \hat{U}_{O_f}$ , and compare them with the locally learned  $\hat{\rho}_{j,O_f}$  in Eq. (4). In principle, scanning  $O_f \in U(m)$  determines whether  $O'$  is correct. In this regard, we have the following Lemma 13.

**Lemma 13.** Given two arbitrary  $m$ -mode states  $\hat{\rho}_1$  and  $\hat{\rho}_2$  that satisfy the following condition:

$$\text{Tr}_{j=1, \dots, m}^{j \neq i} \left[ \hat{U}_{O_f}^\dagger \hat{\rho}_1 \hat{U}_{O_f} \right] \equiv \text{Tr}_{j=1, \dots, m}^{j \neq i} \left[ \hat{U}_{O_f}^\dagger \hat{\rho}_2 \hat{U}_{O_f} \right], \quad (\forall j = 1, \dots, m; \forall O_f \in U(m)), \quad (20)$$

where  $U(m)$  denotes the set of all symplectic orthogonal matrices corresponding to arbitrary  $m$ -mode passive Gaussian operations. Then, we have:

$$\hat{\rho}_1 \equiv \hat{\rho}_2. \quad (21)$$

The concrete proof of Lemma 13 is shown in Supplemental Note 8.

Note that Lemma 13 requires checking all passive transforms with  $O_f \in U(m)$ ; however, we only have access to the reconstructed reduced states in the r.h.s. of Eq. (20) following a search over all possible  $O_f \in \mathcal{S}_{\text{net},O'}$  from the early steps of the generalized GDE protocol. Nevertheless, as  $O'$  has only  $m^2$  independent parameters, we conjecture that going over the  $O_f$ 's among  $\mathcal{S}_{\text{net},O'}$  in Eq. (14) is sufficient for guaranteeing small errors in the local reduced-state test. This conjecture is subject to future study.

### Learning states with the same GE cost

Regarding the states with the same GE cost, we have the following proposition:

**Proposition 14.** (Sample complexity of NGE states): Consider the set of  $m$ -mode pure states  $\mathcal{H}_{m,E}^2$  with a GE cost vector  $\mathcal{R} = (\mathcal{R}_1, \dots, \mathcal{R}_\ell)^T$  satisfying  $\mathcal{R}_f > 7$ . Then, the tomography of such states will take  $M$  copies that satisfy:

$$M \geq \Theta \left[ \frac{1 - \delta}{m \log E} \left( \frac{E}{\epsilon} \right)^{\mathcal{R}_f + 1} \right], \quad (22)$$

$$M \leq \mathcal{O} \left[ \text{poly} \left( \ell^{5\mathcal{R}_f + 9}, E^{2\mathcal{R}_f + 3}, \left( \frac{1}{\epsilon} \right)^{2\mathcal{R}_f + 6}, \log \frac{1}{\delta}, 3^{2\mathcal{R}_f + 2} \right) \right] \quad (23)$$

where  $\delta$  denotes the failure probability and  $\epsilon$  refers to the trace distance between the input and the reconstructed state. Note that we have  $\ell = \mathcal{O}(m)$  by definition.

A detailed proof of Proposition 14 is shown in Supplemental Note 7 C. In addition, it is shown that the sample-complexity scaling is dominated by covariance-matrix estimation when  $\mathcal{R}_f$  is small (e.g.,  $\mathcal{R}_f \leq 7$ ).

### Connection to universality

To produce multi-mode non-Gaussian states, a general approach is to enable inline multi-mode non-Gaussian interactions, which is challenging especially in a network setting. Despite the universality<sup>50</sup> reduction of such interactions into Gaussian operations and single-mode non-Gaussian gates, the required concatenation of inline single-mode non-Gaussian gates and multiple rounds of Gaussian operations remains a conundrum for experimental realization. In this regard, it is intriguing to consider the class of GE states generated from a single round of multi-mode Gaussian interaction from separable local non-Gaussian states. Avoiding the most challenging inline non-Gaussian gates, GE states are more experimentally friendly.

### Related works

So far, various attempts have been made to understand the interplay between entanglement and non-Gaussianity. From the perspective of measurement design, the paradigmatic boson sampling protocol<sup>64</sup> employs passive Gaussian operations and single-photon detectors, demonstrating the potential for scalable photonic quantum computing. More recently, a state-driven resource theory about non-Gaussian correlation has been proposed in ref. 65. Nevertheless, this resource theory is non-convex, hence being operationally constrained. Further, refs. 54,66–68 consider non-Gaussian entanglement based upon whether a state can be mapped to a separable state via a beam-splitter network. In addition to advancing the understanding of GE states, there are also investigations into the implementation of non-Gaussian operations on Gaussian entangled states<sup>69,70</sup>. Lastly, ref. 71 focuses on non-Gaussian entanglement in light-atom interactions and the formulation and resource theory of genuine non-Gaussian entanglement is not studied.

### Data availability

The data generated in this study have been deposited in GitHub<sup>72</sup>.

### Code availability

The theoretical results of the manuscript are reproducible from the analytical formulas and derivations presented therein. Codes for numerical simulation are available in GitHub<sup>72</sup>.

### References

1. Smithey, D., Beck, M., Raymer, M. G. & Faridani, A. Measurement of the Wigner distribution and the density matrix of a light mode using optical homodyne tomography: application to squeezed states and the vacuum. *Phys. Rev. Lett.* **70**, 1244 (1993).
2. Lvovsky, A. I. & Raymer, M. G. Continuous-variable optical quantum-state tomography. *Rev. Mod. Phys.* **81**, 299 (2009).
3. Anshu, A. & Arunachalam, S. A survey on the complexity of learning quantum states. *Nat. Rev. Phys.* **6**, 59 (2024).
4. Eisert, J. et al. Quantum certification and benchmarking. *Nat. Rev. Phys.* **2**, 382 (2020).
5. O'Donnell, R. & Wright, J. Efficient quantum tomography. In *Proceedings of the Forty-Eighth Annual ACM Symposium on Theory of Computing* (eds Wicks, D. & Mansourby, Y.) 899–912 (ACM, New York, NY, USA, 2016).
6. Kueng, R., Rauhut, H. & Terstiege, U. Low rank matrix recovery from rank one measurements. *Appl. Comput. Harmon. Anal.* **42**, 88 (2017).
7. Mele, F. A. et al. Learning quantum states of continuous variable systems. *Nat. Phys.* <https://doi.org/10.1038/s41567-025-03086-2> (2025)
8. Fanizza, M., Rouz e, C. & Fran ca, D. S. Efficient Hamiltonian, structure and trace distance learning of Gaussian states. Preprint at <https://arxiv.org/abs/2411.03163> (2025).
9. Bittel, L., Mele, F. A., Mele, A. A., Tirone, S. & Lami, L. Optimal estimates of trace distance between bosonic Gaussian states and applications to learning. *Quantum* **9**, 1769 (2025).

10. Weedbrook, C. et al. Gaussian quantum information. *Rev. Mod. Phys.* **84**, 621 (2012).
11. Serafini, A. *Quantum Continuous Variables: A Primer of Theoretical Methods* (CRC Press, 2017).
12. Hong, C. K., Ou, Z. Y. & Mandel, L. Measurement of subpicosecond time intervals between two photons by interference. *Phys. Rev. Lett.* **59**, 2044 (1987).
13. Boto, A. N. et al. Quantum interferometric optical lithography: exploiting entanglement to beat the diffraction limit. *Phys. Rev. Lett.* **85**, 2733 (2000).
14. Mitchell, M. W., Lundeen, J. S. & Steinberg, A. M. Super-resolving phase measurements with a multiphoton entangled state. *Nature* **429**, 161 (2004).
15. Aaronson, S. & Arkhipov, A. The computational complexity of linear optics. In *Proceedings of the Forty-Third Annual ACM Symposium on Theory of Computing* (ed. Vadhan, S. P.) 333–342 (ACM, New York, NY, USA, 2011).
16. Zhong, H.-S. et al. Quantum computational advantage using photons. *Science* **370**, 1460 (2020).
17. Madsen, L. S. et al. Quantum computational advantage with a programmable photonic processor. *Nature* **606**, 75 (2022).
18. VanMeter, N. et al. General linear-optical quantum state generation scheme: applications to maximally path-entangled states. *Phys. Rev. As* **76**, 063808 (2007).
19. Parellada, P. V., i Garcia, V. G., Moyano-Fernández, J. J. & Garcia-Escartin, J. C. No-go theorems for photon state transformations in quantum linear optics. *Results Phys.* **54**, 107108 (2023).
20. Parellada, P. V. et al. Lie algebraic invariants in quantum linear optics. Preprint at <https://arxiv.org/abs/2409.12223> (2024).
21. Diring, A. A., Blumenthal, E., Grinberg, A., Jiang, L. & Hacohe-Gourgy, S. Conditional-not displacement: fast multioscillator control with a single qubit. *Phys. Rev. X* **14**, 011055 (2024).
22. Brady, A. J., Eickbusch, A., Singh, S., Wu, J. & Zhuang, Q. Advances in bosonic quantum error correction with Gottesman–Kitaev–Preskill codes: theory, engineering and applications. *Prog. Quantum Electron.* **93**, 100496 (2024).
23. Marian, P. & Marian, T. A. Relative entropy is an exact measure of non-Gaussianity. *Phys. Rev. A* **88**, 012322 (2013).
24. Genoni, M. G., Paris, M. G. & Banaszek, K. Quantifying the non-Gaussian character of a quantum state by quantum relative entropy. *Phys. Rev. A* **78**, 060303 (2008).
25. Genoni, M. G. & Paris, M. G. Quantifying non-gaussianity for quantum information. *Phys. Rev. A* **82**, 052341 (2010).
26. Zhuang, Q., Shor, P. W. & Shapiro, J. H. Resource theory of non-Gaussian operations. *Phys. Rev. A* **97**, 052317 (2018).
27. Takagi, R. & Zhuang, Q. Convex resource theory of non-Gaussianity. *Phys. Rev. A* **97**, 062337 (2018).
28. Albarelli, F., Genoni, M. G., Paris, M. G. & Ferraro, A. Resource theory of quantum non-gaussianity and Wigner negativity. *Phys. Rev. A* **98**, 052350 (2018).
29. Royer, B., Singh, S. & Girvin, S. M. Encoding qubits in multimode grid states. *PRX Quantum* **3**, 010335 (2022).
30. Wu, J., Brady, A. J. & Zhuang, Q. Optimal encoding of oscillators into more oscillators. *Quantum* **7**, 1082 (2023).
31. Conrad, J., Eisert, J. & Arzani, F. Gottesman–Kitaev–Preskill codes: a lattice perspective. *Quantum* **6**, 648 (2022).
32. Brady, A. J., Wu, J. & Zhuang, Q. Safeguarding oscillators and qudits with distributed two-mode squeezing. *Quantum* **8**, 1478 (2024).
33. Gottesman, D., Kitaev, A. & Preskill, J. Encoding a qubit in an oscillator. *Phys. Rev. A* **64**, 012310 (2001).
34. Chitambar, E. & Gour, G. Quantum resource theories. *Rev. Mod. Phys.* **91**, 025001 (2019).
35. Walls, D. F. & Milburn, G. J. *Quantum Opt.* (Springer Science & Business Media, 2007).
36. Flühmann, C. et al. Encoding a qubit in a trapped-ion mechanical oscillator. *Nature* **566**, 513 (2019).
37. Blais, A., Girvin, S. M. & Oliver, W. D. Quantum information processing and quantum optics with circuit quantum electrodynamics. *Nat. Phys.* **16**, 247 (2020).
38. Giovannetti, V., Garcia-Patron, R., Cerf, N. J. & Holevo, A. S. Ultimate classical communication rates of quantum optical channels. *Nat. Photon.* **8**, 796 (2014).
39. Lawrie, B. J., Lett, P. D., Marino, A. M. & Pooser, R. C. Quantum sensing with squeezed light. *ACS Photonics* **6**, 1307 (2019).
40. Ganapathy, D. et al. Broadband quantum enhancement of the LIGO detectors with frequency-dependent squeezing. *Phys. Rev. X* **13**, 041021 (2023).
41. Larsen, M. V., Chamberland, C., Noh, K., Neergaard-Nielsen, J. S. & Andersen, U. L. Fault-tolerant continuous-variable measurement-based quantum computation architecture. *Prx Quantum* **2**, 030325 (2021).
42. Holevo, A. Some statistical problems for quantum Gaussian states. *IEEE Trans. Inf. Theory* **21**, 533 (1975).
43. Holevo, A. S. *Probabilistic and Statistical Aspects of Quantum Theory*, Vol. 1 (Springer Science & Business Media, 2011).
44. Eisert, J., Scheel, S. & Plenio, M. Distilling Gaussian states with Gaussian operations is impossible. *Phys. Rev. Lett.* **89**, 137903 (2002).
45. Giedke, G. & Cirac, J. I. Characterization of Gaussian operations and distillation of Gaussian states. *Phys. Rev. A* **66**, 032316 (2002).
46. Fiurášek, J. Gaussian transformations and distillation of entangled Gaussian states. *Phys. Rev. Lett.* **89**, 137904 (2002).
47. Niset, J., Fiurášek, J. & Cerf, N. J. No-go theorem for Gaussian quantum error correction. *Phys. Rev. Lett.* **102**, 120501 (2009).
48. Banaszek, K. & Wódkiewicz, K. Nonlocality of the Einstein–Podolsky–Rosen state in the Wigner representation. *Phys. Rev. A* **58**, 4345 (1998).
49. Banaszek, K. & Wódkiewicz, K. Testing quantum nonlocality in phase space. *Phys. Rev. Lett.* **82**, 2009 (1999).
50. Lloyd, S. & Braunstein, S. L. Quantum computation over continuous variables. *Phys. Rev. Lett.* **82**, 1784 (1999).
51. Bartlett, S. D. & Sanders, B. C. Universal continuous-variable quantum computation: requirement of optical nonlinearity for photon counting. *Phys. Rev. A* **65**, 042304 (2002).
52. Mari, A., Giovannetti, V. & Holevo, A. S. Quantum state majorization at the output of bosonic Gaussian channels. *Nature Commun.* **5**, 3826 (2014).
53. De Palma, G., Trevisan, D., Giovannetti, V. & Ambrosio, L. Gaussian optimizers for entropic inequalities in quantum information. *J. Math. Phys.* **59**, 081101 (2018).
54. Chabaud, U. & Walschaers, M. Resources for bosonic quantum computational advantage. *Phys. Rev. Lett.* **130**, 090602 (2023).
55. Nielsen, M. A. & Chuang, I. *Quantum Computation and Quantum Information* (Cambridge university press, 2002).
56. Becker, S., Datta, N., Lami, L. & Rouzé, C. Classical shadow tomography for continuous variables quantum systems. *IEEE Trans. Inf. Theory* **70**, 3427–3452 (2024).
57. Mauro D’Ariano, G., Paris, M. G., & Sacchi, M. F. Quantum tomography. In *Advances in Imaging and Electron Physics* Vol. 128 (ed. Hawkes, P. W.) 205–308 [https://doi.org/10.1016/S1076-5670\(03\)80065-4](https://doi.org/10.1016/S1076-5670(03)80065-4) (Elsevier, 2003).
58. Chabaud, U., Douce, T., Grosshans, F., Kashefi, E., & Markham, D. Building trust for continuous variable quantum states. In *15th Conference on the Theory of Quantum Computation, Communication and Cryptography* <https://arxiv.org/abs/arXiv:1905.12700> (2020).
59. Chabaud, U., Grosshans, F., Kashefi, E. & Markham, D. Efficient verification of boson sampling. *Quantum* **5**, 578 (2021).
60. Horodecki, M., Shor, P. W. & Ruskai, M. B. Entanglement breaking channels. *Rev. Math. Phys.* **15**, 629 (2003).

61. Saner, S. et al. Generating arbitrary superpositions of nonclassical quantum harmonic oscillator states. Preprint at <https://arxiv.org/abs/2409.03482> (2024).
  62. Walter, M., Gross, D. & Eisert, J. Multipartite entanglement. In *Quantum Information: From Foundations to Quantum Technology Applications*, (eds Bruß, D. & Leuchs, G.) 293 (Wiley-VCH (John Wiley & Sons), Weinheim, Germany, 2016).
  63. Bădescu, C. & O'Donnell, R. Improved quantum data analysis. In *Proceedings of the 53rd Annual ACM SIGACT Symposium on Theory of Computing* (eds Khuller, S. & Williams, V. V.) 1398–1411 (ACM, New York, NY, United States, 2021).
  64. Knill, E., Laflamme, R. & Milburn, G. J. A scheme for efficient quantum computation with linear optics. *Nature* **409**, 46 (2001).
  65. Park, J., Lee, J., Ji, S.-W. & Nha, H. Quantifying non-Gaussianity of quantum-state correlation. *Phys. Rev. A* **96**, 052324 (2017).
  66. Sperling, J., Perez-Leija, A., Busch, K. & Silberhorn, C. Mode-independent quantum entanglement for light. *Phys. Rev. A* **100**, 062129 (2019).
  67. Chabaud, U. & Mehraban, S. Holomorphic representation of quantum computations. *Quantum* **6**, 831 (2022).
  68. Lopetegui, C. E., Isoard, M., Treppe, N. & Walschaers, M. Detection of mode-intrinsic quantum entanglement. *Optica Quantum* **3**, 312–328 (2025).
  69. Navarrete-Benlloch, C., García-Patrón, R., Shapiro, J. H. & Cerf, N. J. Enhancing quantum entanglement by photon addition and subtraction. *Phys. Rev. A* **86**, 012328 (2012).
  70. Walschaers, M., Fabre, C., Parigi, V. & Treppe, N. Entanglement and Wigner function negativity of multimode non-Gaussian states. *Phys. Rev. Lett.* **119**, 183601 (2017).
  71. Laha, P., Yasir, P. A. & van Loock, P. Genuine non-Gaussian entanglement of light and quantum coherence for an atom from noisy multiphoton spin-boson interactions. *Phys. Rev. Res.* **6**, 033302 (2024).
  72. Zhao, X., Liao, P., Mele, F. A., Chabaud, U. & Zhuang, Q. *Complexity of Quantum Tomography from Genuine non-Gaussian Entanglement* (GitHub, accessed 16 November 2025); <https://github.com/peng-cheng-liao/Complexity-of-quantum-tomography-from-genuine-non-Gaussian-entanglement> (2025).
- Union's Horizon Europe Framework Programme (EIC Pathfinder Challenge project Veriqub) under Grant Agreement No. 101114899 (U.C.).

### Author contributions

Q.Z. proposed the study and supervised the project. X.Z. derived all analytical results, with inputs from all authors. P.L. performed all numerical simulations, with inputs from X.Z. and Q.Z. U.C. and F.A.M. made important contributions to Theorem 2 in the degenerate case, Theorem 3 and Corollary 4. X.Z. and Q.Z. wrote the manuscript, with inputs from all authors.

### Competing interests

The authors declare no competing interests.

### Additional information

**Supplementary information** The online version contains supplementary material available at <https://doi.org/10.1038/s41467-025-67062-3>.

**Correspondence** and requests for materials should be addressed to Xiaobin Zhao or Quntao Zhuang.

**Peer review information** *Nature Communications* thanks the anonymous reviewer(s) for their contribution to the peer review of this work. A peer review file is available.

**Reprints and permissions information** is available at <http://www.nature.com/reprints>

**Publisher's note** Springer Nature remains neutral with regard to jurisdictional claims in published maps and institutional affiliations.

**Open Access** This article is licensed under a Creative Commons Attribution-NonCommercial-NoDerivatives 4.0 International License, which permits any non-commercial use, sharing, distribution and reproduction in any medium or format, as long as you give appropriate credit to the original author(s) and the source, provide a link to the Creative Commons licence, and indicate if you modified the licensed material. You do not have permission under this licence to share adapted material derived from this article or parts of it. The images or other third party material in this article are included in the article's Creative Commons licence, unless indicated otherwise in a credit line to the material. If material is not included in the article's Creative Commons licence and your intended use is not permitted by statutory regulation or exceeds the permitted use, you will need to obtain permission directly from the copyright holder. To view a copy of this licence, visit <http://creativecommons.org/licenses/by-nc-nd/4.0/>.

© The Author(s) 2025

### Acknowledgements

We thank Xun Gao, Haocun Yu, and Changhun Oh for useful comments on an earlier version of this manuscript. This project is supported by NSF 2240641 (Q.Z.), NSF 2350153 (Q.Z.), NSF 2326746 (Q.Z.), ONR N00014-23-1-2296 (Q.Z.), DARPA HR0011-24-9-0362 (Q.Z.), DARPA HR0011-24-9-0453 (Q.Z.), DARPA D24AC00153-02 (Q.Z.), AFOSR MURI FA9550-24-1-0349 (Q.Z.), an unrestricted gift from Google (Q.Z.), PRIN 2022 "Recovering Information in Sloppy QUantum modELs (RISQUE)", code 2022T25TR3, CUP E53D23002400006 (F.A.M.), European Union ERC StG ETQO, Grant Agreement no. 101165230 (F.A.M.) and European